International Journal of
Molecular Sciences

MDPI

Article

Synthesis of Gold-Platinum Core-Shell Nanoparticles Assembled on a Silica Template and Their Peroxidase Nanozyme Properties

Xuan-Hung Pham [1], Van-Khue Tran [2], Eunil Hahm [1], Yoon-Hee Kim [1], Jaehi Kim [1], Wooyeon Kim [1] and Bong-Hyun Jun [1,*]

[1] Department of Bioscience and Biotechnology, Konkuk University, Seoul 05029, Korea; phamricky@gmail.com (X.-H.P.); greenice@konkuk.ac.kr (E.H.); hilite2201@naver.com (Y.-H.K.); susia45@gmail.com (J.K.); buzinga5842@konkuk.ac.kr (W.K.)
[2] VNUK Institute for Research and Executive Education, The University of Danang, Danang 550 000, Vietnam; khue.tran@vnuk.edu.vn
* Correspondence: bjun@konkuk.ac.kr; Tel.: +82-2-450-0521

Abstract: Bimetallic nanoparticles are important materials for synthesizing multifunctional nanozymes. A technique for preparing gold-platinum nanoparticles (NPs) on a silica core template (SiO_2@Au@Pt) using seed-mediated growth is reported in this study. The SiO_2@Au@Pt exhibits peroxidase-like nanozyme activity has several advantages over gold assembled silica core templates (SiO_2@Au@Au), such as stability and catalytic performance. The maximum reaction velocity (V_{max}) and the Michaelis–Menten constants (K_m) were and 2.1×10^{-10} $M^{-1} \cdot s^{-1}$ and 417 μM, respectively. Factors affecting the peroxidase activity, including the quantity of NPs, solution pH, reaction time, and concentration of tetramethyl benzidine, are also investigated in this study. The optimization of SiO_2@Au@Pt NPs for H_2O_2 detection obtained in 0.5 mM TMB; using 5 μg SiO_2@Au@Pt, at pH 4.0 for 15 min incubation. H_2O_2 can be detected in the dynamic liner range of 1.0 to 100 mM with the detection limit of 1.0 mM. This study presents a novel method for controlling the properties of bimetallic NPs assembled on a silica template and increases the understanding of the activity and potential applications of highly efficient multifunctional NP-based nanozymes.

Keywords: gold-platinum bimetallic nanoparticles; nanoparticle; gold-platinum-assembled silica nanostructures; nanozyme; peroxidase-like activity

Citation: Pham, X.-H.; Tran, V.-K.; Hahm, E.; Kim, Y.-H.; Kim, J.; Kim, W.; Jun, B.-H. Synthesis of Gold-Platinum Core-Shell Nanoparticles Assembled on a Silica Template and Their Peroxidase Nanozyme Properties. *Int. J. Mol. Sci.* **2022**, *23*, 6424. https://doi.org/10.3390/ijms23126424

Academic Editor: Ana María Díez-Pascual

Received: 27 April 2022
Accepted: 6 June 2022
Published: 8 June 2022

1. Introduction

Nanozymes, a new functional nanomaterial with enzyme-like catalytic activity, have several advantages when compared with natural enzymes, including high stability in harsh environments, low production costs, large specific surface areas, and customizable catalytic activities based on size, morphology, and composition [1–11]. A series of nanomaterials made from metals, metal oxides, and other materials including Pt [12–14], Au [15–18], Ag [19], Cu [20], Fe_3O_4 [21], CeO_2 [22], MnO_2 [23], Mn_3O_4 [24,25], conducting polymers [26], metal–organic frameworks [27], carbon nanomaterials [28], and single-atom catalysts [29] have been prepared for use as nanozymes. These nanozymes have been used as bio(chemical) sensors, in immunoassays, for drug delivery, and as antibacterial agents [3,12,13,30–34]. While the physical and chemical properties of nanoparticles (NPs) can be adjusted by changing their size, shape, or structure, monometallic NPs are limited by other physical or chemical properties such as size-dependent optical properties, electronic properties, and thermal and catalytic effects that control the chemical compositions of NPs [35].

Several studies have been conducted on bimetallic NPs owing to the increased awareness of the options to adjust their physical and chemical properties. Compared with

monometallic NPs, bimetallic NPs allow a greater adjustment of their magnetic, optical, and catalytic properties via adjustments of their composition and chemical configuration [36]. Bimetallic NPs have unique structure- and composition-dependent properties that allow the optimization of enzyme-like activities more than those of single-metal NPs [37,38]. The Pt family of bimetallic NPs has been developed using various morphologies including core–shell structures, solid solution alloys, intermetallic alloys, and phase-segregated structures. Owing to the synergistic effect caused by the presence of Pt NPs, a super catalyst for electrochemical reactions, which are designed to maximize Pt utilization, tune the energetics, and assemble the geometry of exposed Pt atoms for high catalytic reactivity and selectivity, has been created [39,40]. Bimetallic NPs exhibit various enzyme-like activities including peroxidase, catalase, polyphenol oxidase, ferroxidase, and superoxide dismutase activities [40–44]. Au@Pt bimetallic NPs have intrinsic peroxidase-like activities [45–47], have been studied extensively for electrochemical formic acid and alcohol oxidation, and Pt-rich compositions exhibit enhanced electrocatalytic activity [48,49]. Au@Pt NPs have extensive catalytic properties as they can effectively scavenge superoxide free radicals, H_2O_2, or formic acid, enabling their use in fuel cells, hydrogenation, air purification, anti-aging therapy, and cancer therapy [48,50–52]. However, Pt tends to aggregate in catalytic reactions, resulting in reduced catalytic activity [53].

Au@Ag or Au NPs immobilized on SiO_2 NPs have been developed recently [54–58]. In these nanostructures, the SiO_2 NPs serve as a template and the metal NPs are introduced to the surface using the seed-mediated growth method. Because of the SiO_2 core, the metal NPs assembled on SiO_2 nanostructures are cost-effective, more stable during surface modification, easily separatable from the reaction solution, aggregate less than fine metal NPs, and redisperse into solution with enhanced separation compared with single metal NPs. Furthermore, the effects of various synthesis factors on metal NPs assembled on SiO_2 have been studied using near-infrared surface enhanced Raman scattering nanoprobes for bioimaging [55,56]. However, research regarding the high peroxidase-like activity of the metal NPs assembled on SiO_2 is limited. Therefore, the development of an improved method for preparing metal NPs assembled on SiO_2 templates is needed to enhance peroxidase activity. This study improves the understanding of the activity and applications of highly efficient multifunctional nanozymes.

In this study, gold-platinum NPs are prepared on a silica core template (SiO_2@Au@Pt) using seed-mediated growth combined with the dropping method and utilize it as a nanomaterial to detect hydrogen peroxide (H_2O_2) as a model because H_2O_2 plays an important role in cellular metabolism and in various industry such as food industry, gas sensors, pharmaceuticals, catalysis, environment, and solar energy [59–61]. Therefore, the need to develop a low cost, simple, fast, and sensitive method for monitoring the concentration of H_2O_2 is of practical significance in both industry and academia. The preparation of SiO_2@Au@Pt consists of two steps: tiny Au seeds are embedded on the SiO_2 surface, and the addition of a Pt^{2+} precursor in the presence of ascorbic acid (AA) reductant allows the deposition and growth of the Pt layer. First, a suspension of Au seeds (approximately 2.5 nm) was prepared using tetrakis(hydroxymethyl)phosphonium chloride (THPC) and $HAuCl_4$. Then, the Au seeds were mixed with aminated SiO_2 NPs (approximately 160 nm) overnight to obtain SiO_2@Au seeds, as previously reported [54,55,57,58,62–64]. On the SiO_2@Au seeds, the reduction of Pt^{2+} to Pt(0) was directly induced using AA, a mild reducing agent, in the presence of polyvinylpyrrolidone (PVP). These mildly reducing conditions allow a greater control over the growth of the Pt layer as the reaction proceeds much slower than that in strongly reducing conditions [65]. A low concentration of the Pt^{2+} precursor and AA were added onto the SiO_2@Au seeds in 5 min intervals to enable the precise control of the size of the Pt NPs. After the optimization of synthesis, SiO_2@Au@Pt was used as a peroxidase-like nanomaterial to detect H_2O_2 efficiently.

2. Results and Discussion

2.1. Preparation of Au@Pt NPs-Assembled Silica Nanostructures

The seed-mediated growth from SiO_2@Au seeds was used to prepare the gold-platinum-embedded silica nanospheres (SiO_2@Au@Pt). First, the surface SiO_2 template was assembled using small Au NPs (2.6 ± 0.52 nm) (Figure 1a). Then, 10 mM H_2PtCl_4 and AA solutions were added dropwise into the dispersion of SiO_2@Au seeds to obtain a final Pt^{2+} concentration of 200 μM. The Au@Pt NPs on the surface of the SiO_2 core were bigger (3.6 ± 0.56 nm) than SiO_2@Au seeds. The presence of Pt on the surface of SiO_2@Au was confirmed by the line energy dispersive X-ray (EDS) mapping of SiO_2@Au@Pt (Figures 1b and S1). In Figure 1b, the signal of both Pt and Au elements could obtain in the image. The quantitative EDS analysis in Table S1 of SiO_2@Au@Pt synthesized at 200 μM Pt^{2+} consists of 74.6% Pt and 23.6% Au as mentioned in Table S1.

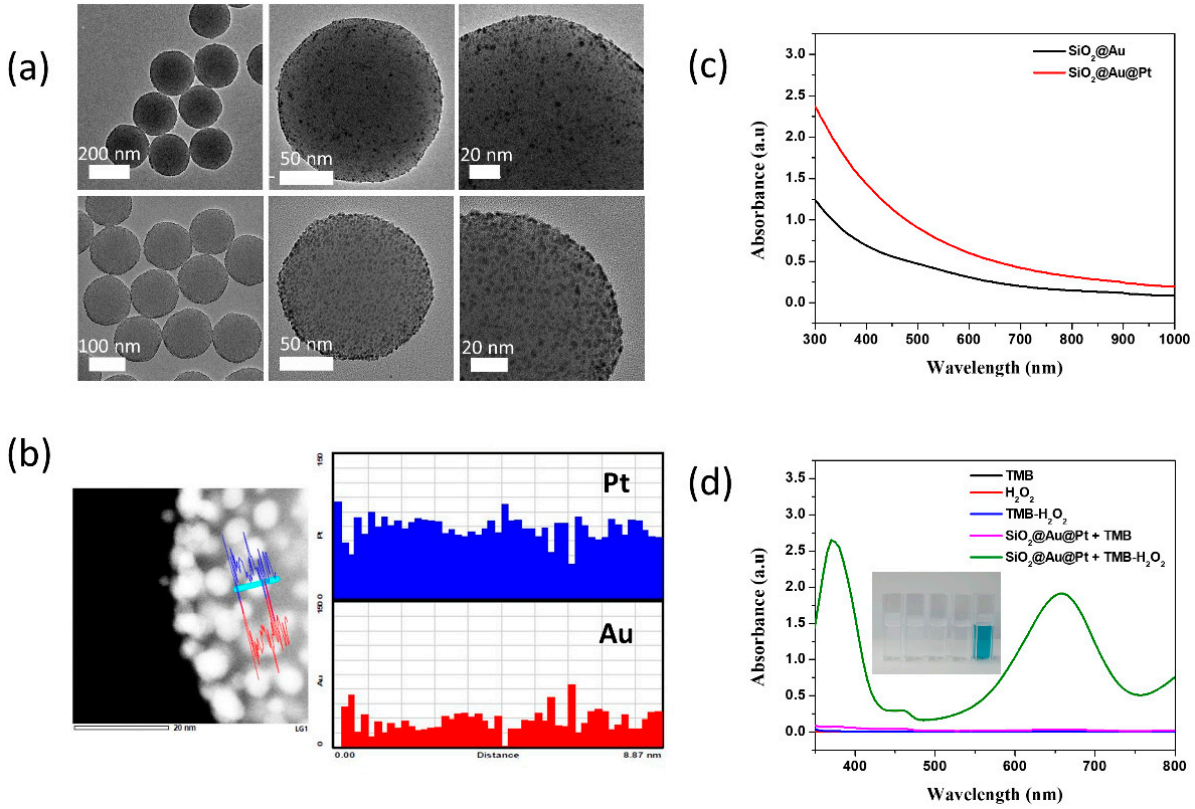

Figure 1. (**a**) Transmission electronic microscopy images of SiO_2@Au seed and gold-platinum-embedded silica nanospheres (SiO_2@Au@Pt) at different magnifications. (**b**) Line energy dispersive X-ray mapping of SiO_2@Au@Pt for Pt and Au elements. (**c**) UV-Vis absorbance spectroscopy of SiO_2@Au seeds and SiO_2@Au@Pt NPs. (**d**) UV-Vis absorbance spectroscopy of SiO_2@Au@Pt in various solutions. The inset shows the colors of the solutions.

The UV-Vis spectroscopy of SiO_2@Au@Pt was conducted when the Pt^{2+} solution was added into the SiO_2@Au seed suspension in the presence of AA. The absorbance intensity of SiO_2@Au showed a slight increase at ~500 nm. This peak was suppressed in the absorbance spectrum of SiO_2@Au@Pt but the spectrum of SiO_2@Au@Pt increased in the UV region (Figure 1c) owing to the Pt layer, consistent with previous results of pure Pt hydrosol [66,67]. The results of TEM, EDS mapping, UV-Vis spectrum of SiO_2@Au@Pt indicated that Pt was deposited to the SiO_2@Au.

2.2. Peroxidase-like Activity of SiO_2@Au@Pt NPs

The peroxidase-like activity of SiO_2@Au@Pt NPs was evaluated using the oxidation reaction of 3,3′,5,5′-tetramethylbenzidine (TMB) substrate prepared in a buffer (pH = 4)

containing TMB or a TMB-H_2O_2 mixture. TMB oxidation involves the exchange of two electrons. When TMB transfers one electron to form TMB^+, the solution changes from colorless to blue. However, TMB^+ is unstable in acidic conditions and must oxidize to TMB^{2+}, forming a yellow solution [68]. In this study, the TMB, H_2O_2, and TMB+H_2O_2 solutions without SiO_2@Au@Pt NPs were colorless and no absorbance peaks were observed at 453 nm (Figure 1d), indicating that there was no peroxidase-like catalytic activity in the absence of SiO_2@Au@Pt. A small absorbance band was observed for the SiO_2@Au@Pt + TMB solution, and a strong absorbance band with peaks at 370 and 652 nm was observed for the SiO_2@Au@Pt + TMB-H_2O_2 solution. The SiO_2@Au@Pt + TMB-H_2O_2 solution changed from blue to yellow and an absorbance band with a peak at 453 nm was observed (Figure S2a). These results indicate that the conversion of TMB to TMB^{2+} was catalyzed by the SiO_2@Au@Pt NPs with H_2O_2, suggesting that SiO_2@Au@Pt NPs has a peroxidase-like activity. To confirm the synergic qualities of SiO_2@Au@Pt, an Au layer was deposited on the surface of the SiO_2@Au seeds using a 200 μM Au^{3+} solution. The peroxidase-like catalytic activity of SiO_2@Au@Pt (5 μg) and SiO_2@Au@Au (5 μg) in TMB and TMB-H_2O_2 solutions was then verified (Figures 2a and S3b).

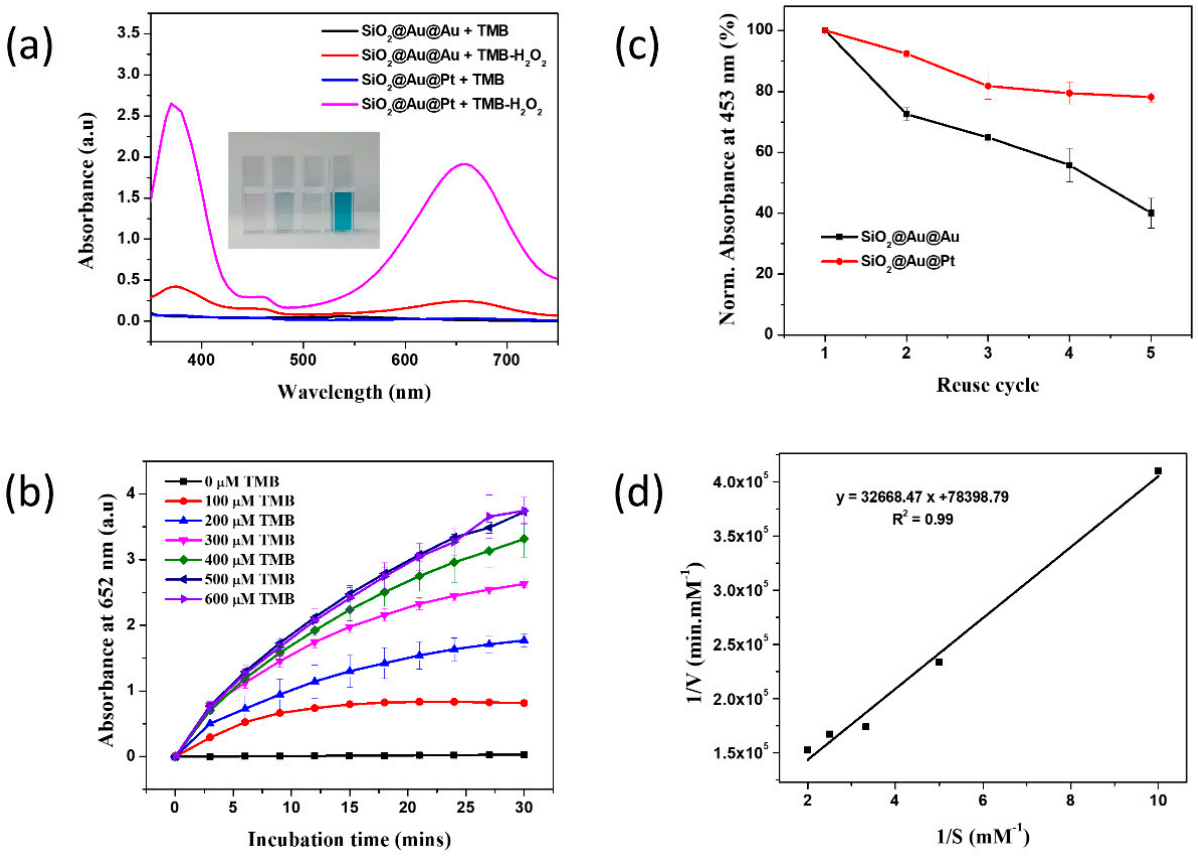

Figure 2. (**a**) UV-Vis absorbance spectroscopy of SiO_2@Au@Pt and SiO_2@Au@Au (5 μg) in TMB and in TMB-H_2O_2 solutions. The inset shows the colors of the solutions. (**b**) The absorbance of recycled SiO_2@Au@Au and SiO_2@Au@Pt is shown in a TMB-H_2O_2 solution. (**c**) UV-Vis absorbance spectroscopy and (**d**) Lineweaver-Burk plot at 652 nm for 5 μg SiO_2@Au@Pt in a TMB-H_2O_2 solution (0–600 μM TMB).

The blue color of the SiO_2@Au@Pt in TMB-H_2O_2 is darker and the absorbance intensity at 370 and 652 nm is stronger than those of the SiO_2@Au@Au suspension. The absorbance intensities of the SiO_2@Au@Pt suspension were 5.7- and 7.7-fold of those of SiO_2@Au@Au at 370 and 652 nm, respectively. Similarly, the absorbance intensity of the SiO_2@Au@Pt suspension at 453 nm was stronger than that of SiO_2@Au@Au (Figure S3b). In addition, the recycling of both SiO_2@Au@Au and SiO_2@Au@Pt in the TMB-H_2O_2 solution at 453 nm was compared when the NPs were reused five times. The absorbance intensity of SiO_2@Au@Au in a TMB-H_2O_2 solution at 453 nm decreased to approximately 40% while that of SiO_2@Au@Pt in a TMB-H_2O_2 solution at 453 nm decreased to 80%. These results indicate that the catalytic ability of SiO_2@Au@Pt is better than that of SiO_2@Au@Au, and that SiO_2@Au@Pt NPs are reusable and separatable from the reaction mixture.

The catalytic performance of SiO_2@Au@Pt NPs at TMB concentrations of 0–600 μM was also investigated as the absorbance intensity at 652 nm in TMB-H_2O_2 every 3 min (Figure 2b). The absorbance intensity of the oxidation of TMB increased as the TMB concentration increased, following Michaelis–Menten behavior. The signal of SiO_2@Au@Pt NPs increased as the TMB concentration increased from 100 to 500 μM and reached saturation at 600 μM. The relationship of the TMB concentration and absorbance intensity at 652 nm after incubation for 180 s was plotted according to the Lineweaver–Burk equation to calculate the maximum reaction velocity (V_{max}) and the Michaelis–Menten constants (K_m) (Figure 2d). The kinetic activity of SiO_2@Au@Pt at various TMB concentrations (100–500 μM) revealed a linear relationship. The K_m was 417 μM and the V_{max} was 2.1×10^{-10} $M^{-1} \cdot s^{-1}$. The K_m of SiO_2@Au@Pt indicates a higher affinity of SiO_2@Au@Pt for TMB compared with that for horseradish peroxidase enzyme (K_m = 438 μM). The K_m of SiO_2@Au@Pt was higher than those of Au NPs (K_m = 123 μM), SiO_2@Au@Au NPs (Km = 60 μM), glucose oxidase-conjugated Au-attached SiO_2 microspheres (K_m = 208 μM), MnO_2 NPs (K_m = 83 μM), and latex-conjugated MnO_2 NPs (K_m = 99 μM). The K_m of SiO_2@Au@Pt was lower than those of Au NPs-decorated porous silica microspheres (K_m = 523 μM) and Prussian-blue-decorated latex NPs (K_m = 2.19 mM) [55]. The V_{max} of SiO_2@Au@Pt was higher than that of SiO_2@Au@Au ($V_{max} = 2.1 \times 10^{-10}$ $M^{-1} \cdot s^{-1}$), indicating that SiO_2@Au@Pt oxidizes TMB at a faster rate than SiO_2@Au@Au. SiO_2@Au@Pt had a comparatively more stable catalytic activity that remained at 80% after five reuses (Figure 2b).

2.3. Effects of Synthesis and Experimental Conditions on the Catalytic Activity of SiO_2@Au@Pt NPs

Various concentrations of the Pt^{2+} precursor (100–400 μM) were added to the SiO_2@Au seeds. The size of Pt increased as the Pt^{2+} concentration increased (Figures 3a and S2). In particularly, the size of Au@Pt synthesized at 100, 200, 300, 400 μM Pt^{2+} were 3.1 ± 0.61; 3.6 ± 0.56; 3.9 ± 0.59; 4.6 ± 0.62 nm, respectively. At a high concentration of Pt^{2+} (>200 μM), the Au@Pt on the SiO_2 surface partly merged. The quantitative EDS analysis of Pt and Au elements on the surface of SiO_2 synthesized at various Pt^{2+} concentration was carried out to investigate the composition of the Au@Pt on the SiO_2 surface and the results were shown in Table S1. All Au@Pt NPs contained both Pt and Au elements, but their Au and Pt components were different. The atomic Pt component increased from 71.59% to 87.07% while the atomic Au component decreased from 28.41 to 12.93% when Pt^{2+} increased from 100 μM to 400 μM. Therefore, the reciprocal of Pt and Au increased from 2.5 (at 100 μM Pt^{2+}) to 6.7 (at 400 μM Pt^{2+}). The results matched to the TEM images, and it indicated that Pt was gradually deposited on the surface of SiO_2@Au.

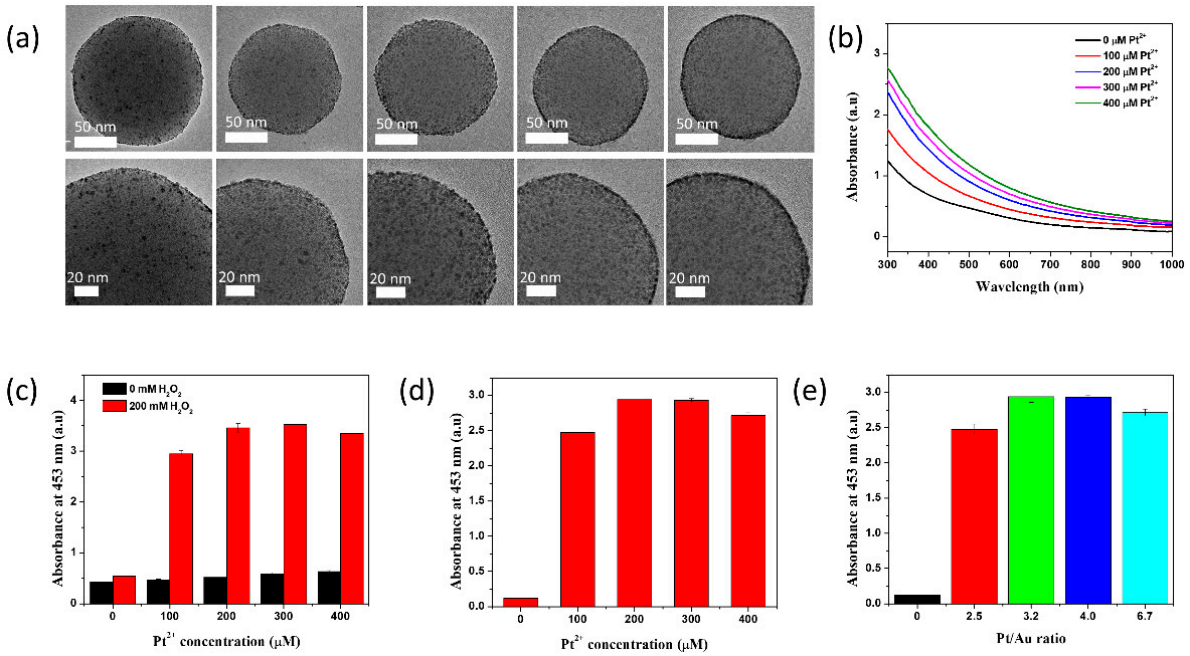

Figure 3. (**a**) TEM images are shown at different magnifications. (**b**) UV–Vis absorbance spectroscopy images of SiO_2@Au@Pt NPs fabricated with various concentrations of Pt^{2+}. (**c**,**d**) Absorbance plots of SiO_2@Au@Pt NPs and (**e**) Effect of Pt/Au ratio on the absorbance at 453 nm in the presence of TMB and H_2O_2 fabricated with various concentrations of Pt^{2+}.

The absorption spectra of SiO_2@Au@Pt were collected (Figure 3b). The absorbance intensity at 300–800 nm increased as the concentration of the Pt^{2+} precursor increased, indicating the formation of larger Au@Pt NPs (Figure S2) that subsequently affected the proximate interparticle distance. The absorbance of the suspension broadened as the size of the Au@Pt NPs increased (Figure S2). The growth of Au@Pt NPs on SiO_2 could be controlled well (Figure 3).

The correlation between the peroxidase-like activity of SiO_2@Au@Pt NPs and the concentration of Pt^{2+} was investigated (Figure 3c). The peroxidase-like activity of SiO_2@Au@Pt NPs synthesized with 100–400 μM Pt^{2+} was estimated using a TMB assay. The SiO_2@Au seeds showed very weak peroxidase-like activity because of the lack of spaces on the SiO_2@Au NPs and the small Au NPs on the SiO_2 template, resulting an insufficient surface area for the catalytic reaction between the Au NPs and the TMB-H_2O_2 mixture [55]. The UV-Vis absorption spectra of all SiO_2@Au@Pt NPs showed an absorbance peak at 453 nm (Figure 3c–e), indicating that all of the SiO_2@Au@Pt NPs had peroxidase-like activity that was dependent on the initial Pt^{2+} concentration.

In contrast, SiO_2@Au@Pt NPs treated with a Pt^{3+} precursor concentration >100 μM had high peroxidase-like activity. As the concentration of Pt^{2+} increased, the size of the Au@Pt NPs on the SiO_2@Au@Pt NPs increased from 3.1 to 4.6 nm, which increased the surface area for reactions between NPs and reactants. Therefore, the catalytic activity of SiO_2@Au@Pt NPs increased as the concentration of the Pt^{2+} precursor increased from 100 to 200 μM because of the formation of sublayers or a monolayer of Pt on the surface of SiO_2@Pt [45,67]. This result consistent with the previous report where the increase of Pt component of Au-Pt led an better catalytic activity because the alloying of Pt with Au can change the electronic structure of Pt, leading the catalytic performance of Au@Pt changes [11,37,69]. Although the Au@Pt NPs grew as the concentration of the Pt^{2+} precursor increased, the peroxidase reaction of SiO_2@Au@Pt treated with >200 μM of the Pt^{2+} precursor did not increase because TMB and H_2O_2 cannot gain access to inner part of the thick Pt layer [66]. It means that the catalytic activities of SiO_2@Au@Pt reached the highest value at the Pt/Au ratio of 3.2 and decreased when Pt^{2+} concentration increased further. Therefore, 200 μM

of Pt^{2+} precursor-treated SiO_2@Au@Pt NPs, which exhibited high peroxidase-like activity, were used in subsequent experiments.

Reaction conditions affect the catalytic activity of nanozymes similarly to the effects of reaction conditions on enzymes [21,70–74]. Therefore, the peroxidase-like activity of different amounts of SiO_2@Au@Pt NPs were investigated at different incubation times, pH values of the buffer solution, and TMB concentrations (Figure 4).

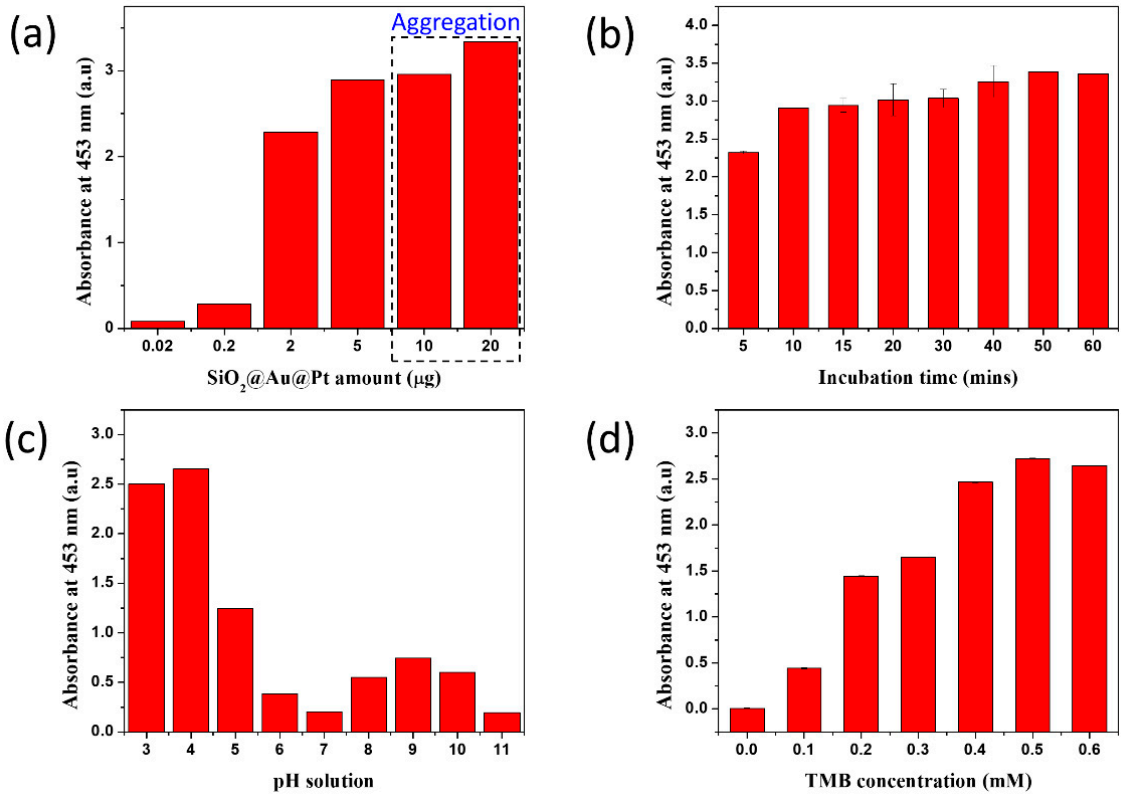

Figure 4. The effects of different conditions on the peroxidase-like catalytic activity of SiO_2@Au@Pt NPs in a mixture of TMB and H_2O_2. (**a**) The amount of SiO_2@Au@Pt, (**b**) incubation time, (**c**) pH of the solution, and (**d**) TMB concentration were varied.

The amount of SiO_2@Au@Pt varied from 0.02 to 20 μg (Figures 4a and S3). The absorbance intensity of SiO_2@Au@Pt in a TMB-H_2O_2 solution at 453 nm increased as the amount of SiO_2@Au@Pt increased from 0.02 to 5 μg. When the amount of SiO_2@Au@Pt increased to >10 μg, the poor solubility of TMB in the aqueous solution resulted in significant aggregation, inducing precipitation with oxidation [55].

The absorbance intensity increased as the incubation time increased from 5 to 15 min (Figures 4b and S4). The absorbance intensity reached saturation after 15 min of incubation.

The highest peroxidase catalytic activity was obtained at a pH of 4.0, at which TMB dissolved maximally and H_2O_2 was the most stable (Figures 4c and S5), which is consistent with the results of previous studies [17,21,75–78].

The absorbance of TMB^{2+} at 453 nm increased as the TMB concentration increased and reached the saturation at 600 μM TMB (Figures 4d and S6).

2.4. Effects of H_2O_2 Concentration on Peroxidase-like Activity of SiO_2@Au@Pt NPs

After optimizing the detection conditions, the absorbance intensity was measured at 0–400 nm for the SiO_2@Au@Pt in 500 μM TMB with various concentrations of H_2O_2 (Figure 5). The yellow color of the 5 μg SiO_2@Au@Pt suspension became darker as the H_2O_2 concentration increased to 200 mM, indicating that more TMB^{2+} was produced as the H_2O_2 concentration increased. The catalytic activity of SiO_2@Au@Pt increased as the

H_2O_2 concentration increased to 200 mM and reached saturation at 300 mM because of aggregation (Figure S7).

A linear curve-fitting procedure was used to calibrate the reaction (Figure 5c). A significant relationship was found between the absorbance intensity at 453 nm and the H_2O_2 concentration from 1.0 to 100 mM (calibration curve: y = 0.0185 x + 0.63285, where x is the H_2O_2 concentration, y is the absorbance intensity at 453 nm, and R^2 = 0.99). The theoretical LOD was 1.0 mM, estimated using the 3sblank criterion. This LOD is higher than the LOD of silver NPs modified cellulose nanowhiskers [79], polyoxometalate [80], $Ce_2(WO_4)_3$, papain [81], Ag-nanoparticle-decorated silica microspheres [82] and magnetic mesoporous silica nanoparticles [83]. These results suggest that this material can be used to detect H_2O_2.

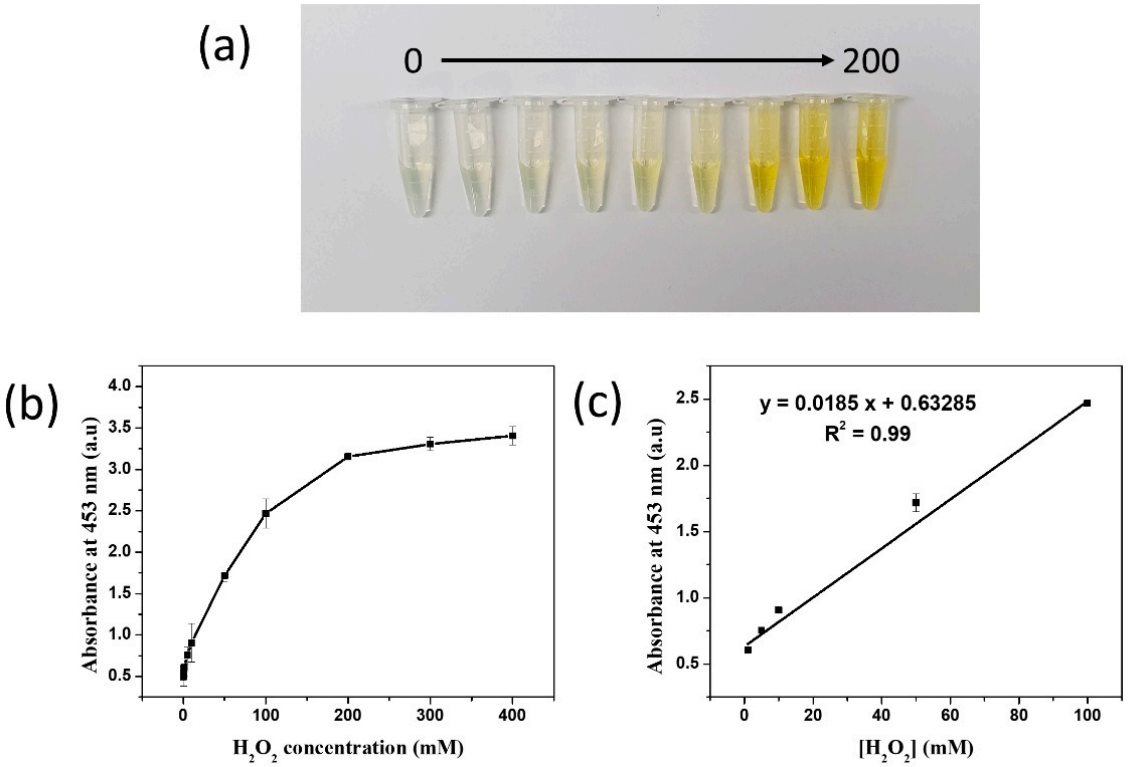

Figure 5. (**a**) Colors of the solutions. (**b**) An absorbance signal plot at 453 nm and (**c**) the dynamic linear range of SiO_2@Au@Pt@Pt at various H_2O_2 concentrations in the presence of 0.5 mM TMB. The optimized conditions were 5 µg SiO_2@Au@Pt@Pt, 0.5 mM TMB, a 15 min incubation period, and a pH of 4.0.

3. Materials and Methods

3.1. Chemicals and Reagents

Tetraethylorthosilicate (TEOS), chloroauric acid ($HAuCl_4$), THPC, chloroplatinic acid (H_2PtCl_6), 3-aminopropyltriethoxysilane (APTS), AA, TMB, and PVP (MW 40,000) were purchased from Sigma-Aldrich (St. Louis, MO, USA). Ammonium hydroxide (NH_4OH, 27%), sodium hydroxide (NaOH), ethyl alcohol (EtOH, 99.9%), and sulfuric acid (H_2SO_4) were obtained from Samchun (Seoul, Korea). H_2O_2 was purchased from Daejung (Siheung, Gyeonggi-do, Korea). Phosphate buffer saline containing 0.1% Tween 20 (PBST, pH 7.4) was obtained from Dynebio (Seongnam, Gyeonggi-do, Korea).

3.2. Characterization

The TEM images of the samples were obtained using a JEM-F200 electron microscope (JEOL, Akishima, Tokyo, Japan) at an accelerated voltage of 200 kV. The UV-Vis spectra of the samples were recorded using an Optizen POP UV/Vis spectrometer (Mecasys, Seoul,

Korea). The samples were centrifuged using a 1730R microcentrifuge (LaboGene, Lyngen, Denmark).

3.3. Synthesis of Gold-Platinum Nanoparticles Assembled on a SiO_2 Nanostructure (SiO_2@Au@Pt NPs)

The SiO_2@Au seed NPs were synthesized as previously reported [54]. Briefly, colloidal Au NPs were prepared from $HAuCl_4$ and THPC. Silica templates (approximately 160 nm) were prepared using the modified Stöber method [84]. The surfaces of 50 mg SiO_2 NPs were modified using amino groups via incubation with 62 µL APTS overnight at 25°C. Animated SiO_2 NPs (2 mg) were incubated with 10 mL colloidal Au (approximately 2.5 nm) for 12 h at 25°C. After the suspension was centrifuged for 10 min at 8500 rpm and washed with EtOH, 2 mg of SiO_2@Au seed NPs were dispersed in 2 mL of 1 mg/mL PVP solution. Subsequently, 200 µL of SiO_2@Au seed (1 mg/mL) suspension was mixed with 9.8 mL of PVP solution. Under stirring, 20 µL of 10 mM $HPtCl_6$ solution (in water, Pt^{2+} precursor) and 40 µL of AA reducing agent (10 mM AA in water) were added to the mixture. The mixture was reacted for 5 min under stirring to convert Pt^{2+} to Pt(0). The same volumes of Pt^{2+} precursor and AA were added every 5 min to obtain the desired concentration of Pt^{2+}. The SiO_2@Au@Pt NPs were then carefully washed with EtOH several times using centrifugation at 8500 rpm for 10 min. The washed SiO_2@Au@Pt NPs were redispersed in 0.1% PBST solution (1 mL) to obtain a 0.2 mg/mL SiO_2@Au@Pt NP suspension.

3.4. Peroxidase-like Activity of SiO_2@Au@Pt NPs

To verify the peroxidase-like catalytic activity of SiO_2@Au@Pt NPs, TMB solution (6 mM in EtOH, 100 µL), the SiO_2@Au@Pt NPs suspension (100 µL) synthesized with 100, 200, 300, and 400 µM Pt^{2+}, and freshly prepared H_2O_2 solution (2 M in pH 4 buffer, 100 µL) were added to 700 µL of buffer (pH = 4.0). Then, the mixture was incubated at 25°C for 15 min. To terminate the reaction, 1 M H_2SO_4 solution (500 µL) was added to each mixture and the resulting mixture was incubated at 25°C for 10 min. The absorbances of the suspensions were measured at 300–1,000 nm using a UV-Vis spectrometer.

3.5. Peroxidase-like Activity of SiO_2@Au@Pt in Various Reaction Conditions

3.5.1. Amount of SiO_2@Au@Pt NPs

A mixture of 6 mM TMB solution in EtOH (100 µL), 2 M H_2O_2 (100 µL), and 700 µL buffer (pH = 4) was added to 100 µL PBST containing 0, 0.2, 2, 5, 10, or 20 µg of SiO_2@Au@Pt. The resulting solution was incubated at 25 °C for 15 min, then terminated with 1 M H_2SO_4 (500 µL). The absorbances were measured at 453 nm using a UV-Vis spectrometer.

3.5.2. Reaction Time

A mixture of a 6 mM TMB (100 µL), a SiO_2@Au@Pt NP suspension (0.05 mg/mL, 100 µL), and 2 M H_2O_2 (100 µL) was added to 700 µL buffer (pH = 4) then incubated at 25°C for various incubation times. The mixture was terminated using 1 M H_2SO_4 (500 µM). The absorbances of the mixtures were measured at 453 nm using a UV-Vis spectrometer.

3.5.3. PH Value of the Buffer

A mixture containing 6 mM TMB (100 µL), a SiO_2@Au@Pt NP suspension (0.05 mg/mL, 100 µL), and 2 M H_2O_2 (100 µL) was added to 700 µL of buffer at a pH range from 3.0 to 11.0. The mixture was incubated for 15 min and terminated using 1 M H_2SO_4 (500 µL). The absorbances of the mixtures were measured at 453 nm using a UV-Vis spectrometer.

3.5.4. TMB Concentration

A mixture containing 700 µM buffer (pH 4.0), 2 M H_2O_2 (100 µL), and 0.05 mg/mL SiO_2@Au@Pt suspension (100 µL) was added to various concentrations of TMB (1, 2, 3, 4, 5, and 6 mM). The final TMB concentration in the reaction mixture was 0.1, 0.2, 0.3, 0.4, 0.5, and 0.6 mM. After incubating the mixture for 15 min, the reaction was terminated using

1 M H_2SO_4 (500 µL). The absorbances of the mixtures were measured at 453 nm using a UV-Vis spectrometer.

4. Conclusions

In summary, SiO_2@Au@Pt NPs were successfully synthesized using the seed-mediated growth method under mild conditions. Compared with SiO_2@Au@Au, the SiO_2@Au@Pt NPs exhibited more synergic and stable catalytic abilities that remained at 80% after five uses of 5 µg SiO_2@Au@Pt NPs. In addition, the peroxidase-like activity of SiO_2@Au@Pt NPs under various conditions such as the amount of SiO_2@Au@Pt NPs, pH of the buffer solution, incubation time, and TMB concentration were also investigated, revealing optimized conditions of 5 µg SiO_2@Au@Pt at pH 4.0, with 15 min of incubation in the presence of 500 µM TMB. SiO_2@Au@Pt was used to detect H_2O_2. The dynamic linear range was obtained from 1 to 100 mM, with an LOD of 1.0 mM. Therefore, this study suggests novel uses of bimetallic metal-assembled silica nanostructures in various fields and provides a suitable method for the development of nanoparticle-based multi-functional nanozymes.

Supplementary Materials: The following supporting information can be downloaded at: https://www.mdpi.com/article/10.3390/ijms23126424/s1.

Author Contributions: Conceptualization, X.-H.P., V.-K.T., and B.-H.J.; methodology, V.-K.T. and X.-H.P.; investigation, W.K. and Y.-H.K.; formal analysis, X.-H.P., E.H., and J.K.; writing—original draft preparation, V.-K.T., X.-H.P., and E.H.; writing—review and editing, J.K. and B.-H.J.; supervisor, B.-H.J. All authors have read and agreed to the published version of the manuscript.

Funding: This research was funded by the KU Research Professor Program of Konkuk University and funded by the Ministry of Science and ICT (NRF-2022R1A2C2012883).

Institutional Review Board Statement: Not applicable.

Informed Consent Statement: Not applicable.

Data Availability Statement: Data is available in the manuscript and supporting information.

Acknowledgments: The authors are grateful for the financial support from the NRF of Korea. Further, the authors give thanks for the financial support from Konkuk University.

Conflicts of Interest: The authors declare no conflict of interest.

References

1. Ragg, R.; Tahir, M.N.; Tremel, W. Solids Go Bio: Inorganic Nanoparticles as Enzyme Mimics. *Eur. J. Inorg. Chem.* **2016**, *2016*, 1906–1915. [CrossRef]
2. Zhou, Y.; Liu, B.; Yang, R.; Liu, J. Filling in the Gaps between Nanozymes and Enzymes: Challenges and Opportunities. *Bioconjug. Chem.* **2017**, *28*, 2903–2909. [CrossRef] [PubMed]
3. Wang, X.; Hu, Y.; Wei, H. Nanozymes in bionanotechnology: From sensing to therapeutics and beyond. *Inorg. Chem. Front.* **2016**, *3*, 41–60. [CrossRef]
4. Wu, J.; Li, S.; Wei, H. Multifunctional nanozymes: Enzyme-like catalytic activity combined with magnetism and surface plasmon resonance. *Nanoscale Horiz.* **2018**, *3*, 367–382. [CrossRef] [PubMed]
5. Wu, J.; Li, S.; Wei, H. Integrated nanozymes: Facile preparation and biomedical applications. *Chem. Commun.* **2018**, *54*, 6520–6530. [CrossRef]
6. Jiang, D.; Ni, D.; Rosenkrans, Z.T.; Huang, P.; Yan, X.; Cai, W. Nanozyme: New horizons for responsive biomedical applications. *Chem. Soc. Rev.* **2019**, *48*, 3683–3704. [CrossRef]
7. Wei, H.; Wang, E. Nanomaterials with enzyme-like characteristics (nanozymes): Next-generation artificial enzymes. *Chem. Soc. Rev.* **2013**, *42*, 6060–6093. [CrossRef]
8. Gao, L.; Fan, K.; Yan, X. Iron Oxide Nanozyme: A Multifunctional Enzyme Mimetic for Biomedical Applications. *Theranostics* **2017**, *7*, 3207–3227. [CrossRef]
9. Wu, J.; Wang, X.; Wang, Q.; Lou, Z.; Li, S.; Zhu, Y.; Qin, L.; Wei, H. Nanomaterials with enzyme-like characteristics (nanozymes): Next-generation artificial enzymes (II). *Chem. Soc. Rev.* **2019**, *48*, 1004–1076. [CrossRef]
10. Wang, X.; Gao, X.J.; Qin, L.; Wang, C.; Song, L.; Zhou, Y.-N.; Zhu, G.; Cao, W.; Lin, S.; Zhou, L.; et al. eg occupancy as an effective descriptor for the catalytic activity of perovskite oxide-based peroxidase mimics. *Nat. Commun.* **2019**, *10*, 704. [CrossRef]
11. Zhang, K.; Hu, X.; Liu, J.; Yin, J.-J.; Hou, S.; Wen, T.; He, W.; Ji, Y.; Guo, Y.; Wang, Q.; et al. Formation of PdPt Alloy Nanodots on Gold Nanorods: Tuning Oxidase-like Activities via Composition. *Langmuir* **2011**, *27*, 2796–2803. [CrossRef] [PubMed]

12. Zhang, Y.; Wang, F.; Liu, C.; Wang, Z.; Kang, L.; Huang, Y.; Dong, K.; Ren, J.; Qu, X. Nanozyme Decorated Metal–Organic Frameworks for Enhanced Photodynamic Therapy. *ACS Nano* **2018**, *12*, 651–661. [CrossRef] [PubMed]
13. Wang, X.; Qin, L.; Zhou, M.; Lou, Z.; Wei, H. Nanozyme Sensor Arrays for Detecting Versatile Analytes from Small Molecules to Proteins and Cells. *Anal. Chem.* **2018**, *90*, 11696–11702. [CrossRef]
14. Han, L.; Zhang, H.; Li, F. Bioinspired Nanozymes with pH-Independent and Metal Ions-Controllable Activity: Field-Programmable Logic Conversion of Sole Logic Gate System. *Part. Part. Syst. Charact.* **2018**, *35*, 1800207. [CrossRef]
15. Zhang, Z.; Wang, J.; Nie, X.; Wen, T.; Ji, Y.; Wu, X.; Zhao, Y.; Chen, C. Near infrared laser-induced targeted cancer therapy using thermoresponsive polymer encapsulated gold nanorods. *J. Am. Chem. Soc.* **2014**, *136*, 7317–7326. [CrossRef] [PubMed]
16. Wang, F.; Ju, E.; Guan, Y.; Ren, J.; Qu, X. Light-Mediated Reversible Modulation of ROS Level in Living Cells by Using an Activity-Controllable Nanozyme. *Small* **2017**, *13*, 1603051. [CrossRef]
17. He, W.; Zhou, Y.-T.; Wamer, W.G.; Hu, X.; Wu, X.; Zheng, Z.; Boudreau, M.D.; Yin, J.-J. Intrinsic catalytic activity of Au nanoparticles with respect to hydrogen peroxide decomposition and superoxide scavenging. *Biomaterials* **2013**, *34*, 765–773. [CrossRef]
18. Das, R.; Dhiman, A.; Kapil, A.; Bansal, V.; Sharma, T.K. Aptamer-mediated colorimetric and electrochemical detection of Pseudomonas aeruginosa utilizing peroxidase-mimic activity of gold NanoZyme. *Anal. Bioanal. Chem.* **2019**, *411*, 1229–1238. [CrossRef]
19. Pham, X.-H.; Seong, B.; Bock, S.; Hahm, E.; Huynh, K.-H.; Kim, Y.-H.; Kim, W.; Kim, J.; Kim, D.-E.; Jun, B.-H. Nonenzymatic Hydrogen Peroxide Detection Using Surface-Enhanced Raman Scattering of Gold–Silver Core–Shell-Assembled Silica Nanostructures. *Nanomaterials* **2021**, *11*, 2748. [CrossRef]
20. Walther, R.; Winther, A.K.; Fruergaard, A.S.; van den Akker, W.; Sørensen, L.; Nielsen, S.M.; Jarlstad Olesen, M.T.; Dai, Y.; Jeppesen, H.S.; Lamagni, P.; et al. Identification and Directed Development of Non-Organic Catalysts with Apparent Pan-Enzymatic Mimicry into Nanozymes for Efficient Prodrug Conversion. *Angew. Chem. Int. Ed.* **2019**, *58*, 278–282. [CrossRef]
21. Gao, L.; Zhuang, J.; Nie, L.; Zhang, J.; Zhang, Y.; Gu, N.; Wang, T.; Feng, J.; Yang, D.; Perrett, S.; et al. Intrinsic peroxidase-like activity of ferromagnetic nanoparticles. *Nat. Nanotechnol.* **2007**, *2*, 577–583. [CrossRef] [PubMed]
22. Bhagat, S.; Srikanth Vallabani, N.V.; Shutthanandan, V.; Bowden, M.; Karakoti, A.S.; Singh, S. Gold core/ceria shell-based redox active nanozyme mimicking the biological multienzyme complex phenomenon. *J. Colloid Interface Sci.* **2018**, *513*, 831–842. [CrossRef] [PubMed]
23. Huang, Y.; Liu, Z.; Liu, C.; Ju, E.; Zhang, Y.; Ren, J.; Qu, X. Self-Assembly of Multi-nanozymes to Mimic an Intracellular Antioxidant Defense System. *Angew. Chem. Int. Ed.* **2016**, *55*, 6646–6650. [CrossRef] [PubMed]
24. Singh, N.; Savanur, M.A.; Srivastava, S.; D'Silva, P.; Mugesh, G. A Redox Modulatory Mn3O4 Nanozyme with Multi-Enzyme Activity Provides Efficient Cytoprotection to Human Cells in a Parkinson's Disease Model. *Angew. Chem. Int. Ed.* **2017**, *56*, 14267–14271. [CrossRef] [PubMed]
25. Singh, N.; Geethika, M.; Eswarappa, S.M.; Mugesh, G. Manganese-Based Nanozymes: Multienzyme Redox Activity and Effect on the Nitric Oxide Produced by Endothelial Nitric Oxide Synthase. *Chem. A Eur. J.* **2018**, *24*, 8393–8403. [CrossRef]
26. Yang, Z.; Wang, C.; Lu, X. Conducting polymer-based peroxidase mimics: Synthesis, synergistic enhanced properties and applications. *Sci. China Mater.* **2018**, *61*, 653–670. [CrossRef]
27. Zheng, H.-Q.; Liu, C.-Y.; Zeng, X.-Y.; Chen, J.; Lü, J.; Lin, R.-G.; Cao, R.; Lin, Z.-J.; Su, J.-W. MOF-808: A Metal–Organic Framework with Intrinsic Peroxidase-Like Catalytic Activity at Neutral pH for Colorimetric Biosensing. *Inorg. Chem.* **2018**, *57*, 9096–9104. [CrossRef]
28. Garg, B.; Bisht, T. Carbon Nanodots as Peroxidase Nanozymes for Biosensing. *Molecules* **2016**, *21*, 1653. [CrossRef]
29. Zhang, X.; Li, G.; Chen, G.; Wu, D.; Zhou, X.; Wu, Y. Single-atom nanozymes: A rising star for biosensing and biomedicine. *Coordin. Chem. Rev.* **2020**, *418*, 213376. [CrossRef]
30. Huang, Y.; Ren, J.; Qu, X. Nanozymes: Classification, Catalytic Mechanisms, Activity Regulation, and Applications. *Chem. Rev.* **2019**, *119*, 4357–4412. [CrossRef]
31. Sindhu, R.K.; Najda, A.; Kaur, P.; Shah, M.; Singh, H.; Kaur, P.; Cavalu, S.; Jaroszuk-Sierocińska, M.; Rahman, M.H. Potentiality of Nanoenzymes for Cancer Treatment and Other Diseases: Current Status and Future Challenges. *Materials* **2021**, *14*, 5965. [CrossRef] [PubMed]
32. Wang, P.; Wang, T.; Hong, J.; Yan, X.; Liang, M. Nanozymes: A New Disease Imaging Strategy. *Front. Bioeng. Biotechnol.* **2020**, *8*, 15. [CrossRef] [PubMed]
33. Wang, Q.; Wei, H.; Zhang, Z.; Wang, E.; Dong, S. Nanozyme: An emerging alternative to natural enzyme for biosensing and immunoassay. *Trends Anal. Chem. TrAC* **2018**, *105*, 218–224. [CrossRef]
34. Das, B.; Franco, J.L.; Logan, N.; Balasubramanian, P.; Kim, M.I.; Cao, C. Nanozymes in Point-of-Care Diagnosis: An Emerging Futuristic Approach for Biosensing. *Nano-Micro Lett.* **2021**, *13*, 193. [CrossRef] [PubMed]
35. Sharma, G.; Kumar, A.; Sharma, S.; Naushad, M.; Prakash Dwivedi, R.; Alothman, Z.A.; Mola, G.T. Novel development of nanoparticles to bimetallic nanoparticles and their composites: A review. *J. King Saud Univ. Sci.* **2019**, *31*, 257–269. [CrossRef]
36. Langlois, C.; Li, Z.L.; Yuan, J.; Alloyeau, D.; Nelayah, J.; Bochicchio, D.; Ferrando, R.; Ricolleau, C. Transition from core–shell to Janus chemical configuration for bimetallic nanoparticles. *Nanoscale* **2012**, *4*, 3381–3388. [CrossRef]
37. Hu, X.; Saran, A.; Hou, S.; Wen, T.; Ji, Y.; Liu, W.; Zhang, H.; He, W.; Yin, J.-J.; Wu, X. Au@PtAg core/shell nanorods: Tailoring enzyme-like activities via alloying. *RSC Adv.* **2013**, *3*, 6095–6105. [CrossRef]

38. Cai, S.; Qi, C.; Li, Y.; Han, Q.; Yang, R.; Wang, C. PtCo bimetallic nanoparticles with high oxidase-like catalytic activity and their applications for magnetic-enhanced colorimetric biosensing. *J. Mater. Chem. B* **2016**, *4*, 1869–1877. [CrossRef]
39. Lapp, A.S.; Duan, Z.; Marcella, N.; Luo, L.; Genc, A.; Ringnalda, J.; Frenkel, A.I.; Henkelman, G.; Crooks, R.M. Experimental and Theoretical Structural Investigation of AuPt Nanoparticles Synthesized Using a Direct Electrochemical Method. *J. Am. Chem. Soc.* **2018**, *140*, 6249–6259. [CrossRef]
40. Gawande, M.B.; Goswami, A.; Asefa, T.; Guo, H.; Biradar, A.V.; Peng, D.-L.; Zboril, R.; Varma, R.S. Core–shell nanoparticles: Synthesis and applications in catalysis and electrocatalysis. *Chem. Soc. Rev.* **2015**, *44*, 7540–7590. [CrossRef]
41. He, W.; Wamer, W.; Xia, Q.; Yin, J.-j.; Fu, P.P. Enzyme-Like Activity of Nanomaterials. *J. Environ. Sci. Health Part C* **2014**, *32*, 186–211. [CrossRef] [PubMed]
42. Liu, J.; Jiang, X.; Wang, L.; Hu, Z.; Wen, T.; Liu, W.; Yin, J.; Chen, C.; Wu, X. Ferroxidase-like activity of Au nanorod/Pt nanodot structures and implications for cellular oxidative stress. *Nano Res.* **2015**, *8*, 4024–4037. [CrossRef]
43. Liu, Y.; Wu, H.; Chong, Y.; Wamer, W.G.; Xia, Q.; Cai, L.; Nie, Z.; Fu, P.P.; Yin, J.-J. Platinum Nanoparticles: Efficient and Stable Catechol Oxidase Mimetics. *ACS Appl. Mater. Interfaces* **2015**, *7*, 19709–19717. [CrossRef] [PubMed]
44. Zhou, Y.-T.; He, W.; Wamer, W.G.; Hu, X.; Wu, X.; Lo, Y.M.; Yin, J.-J. Enzyme-mimetic effects of gold@platinum nanorods on the antioxidant activity of ascorbic acid. *Nanoscale* **2013**, *5*, 1583–1591. [CrossRef]
45. Wu, Q.; Li, Y.; Xian, H.; Xu, C.; Wang, L.; Chen, Z. Ultralow Pt-loading bimetallic nanoflowers: Fabrication and sensing applications. *Nanotechnology* **2012**, *24*, 25501. [CrossRef]
46. Tseng, C.-W.; Chang, H.-Y.; Chang, J.-Y.; Huang, C.-C. Detection of mercury ions based on mercury-induced switching of enzyme-like activity of platinum/gold nanoparticles. *Nanoscale* **2012**, *4*, 6823–6830. [CrossRef]
47. Li, X.-R.; Xu, M.-C.; Chen, H.-Y.; Xu, J.-J. Bimetallic Au@Pt@Au core–shell nanoparticles on graphene oxide nanosheets for high-performance H2O2 bi-directional sensing. *J. Mater. Chem. B* **2015**, *3*, 4355–4362. [CrossRef]
48. Li, D.; Meng, F.; Wang, H.; Jiang, X.; Zhu, Y. Nanoporous AuPt alloy with low Pt content: A remarkable electrocatalyst with enhanced activity towards formic acid electro-oxidation. *Electrochim. Acta* **2016**, *190*, 852–861. [CrossRef]
49. Suntivich, J.; Xu, Z.; Carlton, C.E.; Kim, J.; Han, B.; Lee, S.W.; Bonnet, N.; Marzari, N.; Allard, L.F.; Gasteiger, H.A.; et al. Surface Composition Tuning of Au–Pt Bimetallic Nanoparticles for Enhanced Carbon Monoxide and Methanol Electro-oxidation. *J. Am. Chem. Soc.* **2013**, *135*, 7985–7991. [CrossRef]
50. Kajita, M.; Hikosaka, K.; Iitsuka, M.; Kanayama, A.; Toshima, N.; Miyamoto, Y. Platinum nanoparticle is a useful scavenger of superoxide anion and hydrogen peroxide. *Free Radic. Res.* **2007**, *41*, 615–626. [CrossRef]
51. Kim, J.; Takahashi, M.; Shimizu, T.; Shirasawa, T.; Kajita, M.; Kanayama, A.; Miyamoto, Y. Effects of a potent antioxidant, platinum nanoparticle, on the lifespan of Caenorhabditis elegans. *Mech. Ageing Dev.* **2008**, *129*, 322–331. [CrossRef] [PubMed]
52. Hamasaki, T.; Kashiwagi, T.; Imada, T.; Nakamichi, N.; Aramaki, S.; Toh, K.; Morisawa, S.; Shimakoshi, H.; Hisaeda, Y.; Shirahata, S. Kinetic analysis of superoxide anion radical-scavenging and hydroxyl radical-scavenging activities of platinum nanoparticles. *Langmuir* **2008**, *24*, 7354–7364. [CrossRef] [PubMed]
53. Li, J.; Xu, K.; Chen, Y.; Zhao, J.; Du, P.; Zhang, L.; Zhang, Z.; Lu, X. Pt Nanoparticles Anchored on NH2-MIL-101 with Efficient Peroxidase-Like Activity for Colorimetric Detection of Dopamine. *Chemosensors* **2021**, *9*, 140. [CrossRef]
54. Seong, B.; Bock, S.; Hahm, E.; Huynh, K.-H.; Kim, J.; Lee, S.H.; Pham, X.-H.; Jun, B.-H. Synthesis of Densely Immobilized Gold-Assembled Silica Nanostructures. *Int. J. Mol. Sci.* **2021**, *22*, 2543. [CrossRef] [PubMed]
55. Seong, B.; Kim, J.; Kim, W.; Lee, S.H.; Pham, X.-H.; Jun, B.-H. Synthesis of Finely Controllable Sizes of Au Nanoparticles on a Silica Template and Their Nanozyme Properties. *Int. J. Mol. Sci.* **2021**, *22*, 10382. [CrossRef]
56. Bock, S.; Choi, Y.-S.; Kim, M.; Yun, Y.; Pham, X.-H.; Kim, J.; Seong, B.; Kim, W.; Jo, A.; Ham, K.-M.; et al. Highly sensitive near-infrared SERS nanoprobes for in vivo imaging using gold-assembled silica nanoparticles with controllable nanogaps. *J. Nanobiotechnol.* **2022**, *20*, 130. [CrossRef]
57. Pham, X.-H.; Hahm, E.; Kang, E.; Ha, Y.N.; Lee, S.H.; Rho, W.-Y.; Lee, Y.-S.; Jeong, D.H.; Jun, B.-H. Gold-silver bimetallic nanoparticles with a Raman labeling chemical assembled on silica nanoparticles as an internal-standard-containing nanoprobe. *J. Alloys Compd.* **2019**, *779*, 360–366. [CrossRef]
58. Pham, X.-H.; Hahm, E.; Huynh, K.-H.; Son, B.S.; Kim, H.-M.; Jeong, D.H.; Jun, B.-H. 4-Mercaptobenzoic Acid Labeled Gold-Silver-Alloy-Embedded Silica Nanoparticles as an Internal Standard Containing Nanostructures for Sensitive Quantitative Thiram Detection. *Int. J. Mol. Sci.* **2019**, *20*, 4841. [CrossRef]
59. Yang, H.; Wang, J.; Li, X.; Zhang, L.; Yu, H.; Zhang, L.; Ge, S.; Yu, J.; Zhang, Y. Self-Circulation Oxygen–Hydrogen Peroxide–Oxygen System for Ultrasensitive Cathode Photoelectrochemical Bioassay Using a Stacked Sealed Paper Device. *ACS Appl. Mater. Interfaces* **2021**, *13*, 19793–19802. [CrossRef]
60. Liu, H.; Weng, L.; Yang, C. A review on nanomaterial-based electrochemical sensors for H2O2, H2S and NO inside cells or released by cells. *Microchim. Acta* **2017**, *184*, 1267–1283. [CrossRef]
61. Elias, H.; Vayssié, S. Reactive Peroxo Compounds Generated in Situ from Hydrogen Peroxide: Kinetics and Catalytic Application in Oxidation Processes. In *Peroxide Chemistry*; Wiley: Hoboken, NJ, USA, 2000; pp. 128–138. [CrossRef]
62. Shim, S.; Pham, X.-H.; Cha, M.G.; Lee, Y.-S.; Jeong, D.H.; Jun, B.-H. Size effect of gold on Ag-coated Au nanoparticle-embedded silica nanospheres. *RSC Adv.* **2016**, *6*, 48644–48650. [CrossRef]

63. Pham, X.-H.; Lee, M.; Shim, S.; Jeong, S.; Kim, H.-M.; Hahm, E.; Lee, S.H.; Lee, Y.-S.; Jeong, D.H.; Jun, B.-H. Highly sensitive and reliable SERS probes based on nanogap control of a Au-Ag alloy on silica nanoparticles. *RSC Adv.* **2017**, *7*, 7015–7021. [CrossRef]
64. Pham, X.-H.; Hahm, E.; Kang, E.; Son, B.S.; Ha, Y.; Kim, H.-M.; Jeong, D.H.; Jun, B.-H. Control of Silver Coating on Raman Label Incorporated Gold Nanoparticles Assembled Silica Nanoparticles. *Int. J. Mol. Sci.* **2019**, *20*, 1258. [CrossRef] [PubMed]
65. Grzelczak, M.; Pérez-Juste, J.; Mulvaney, P.; Liz-Marzán, L.M. Shape control in gold nanoparticle synthesis. *Chem. Soc. Rev.* **2008**, *37*, 1783–1791. [CrossRef] [PubMed]
66. Feng, R.; Li, M.; Liu, J. Synthesis of core–shell Au@Pt nanoparticles supported on Vulcan XC-72 carbon and their electrocatalytic activities for methanol oxidation. *Colloid Surf. A Physicochem. Eng. Asp.* **2012**, *406*, 6–12. [CrossRef]
67. Kristian, N.; Yan, Y.; Wang, X. Highly efficient submonolayer Pt-decorated Au nano-catalysts for formic acid oxidation. *Chem. Commun.* **2008**, *3*, 353–355. [CrossRef]
68. Josephy, P.D.; Eling, T.; Mason, R.P. The horseradish peroxidase-catalyzed oxidation of 3,5,3′,5′-tetramethylbenzidine. Free radical and charge-transfer complex intermediates. *J. Biol. Chem.* **1982**, *257*, 3669–3675. [CrossRef]
69. He, W.; Han, X.; Jia, H.; Cai, J.; Zhou, Y.; Zheng, Z. AuPt Alloy Nanostructures with Tunable Composition and Enzyme-like Activities for Colorimetric Detection of Bisulfide. *Sci. Rep.* **2017**, *7*, 40103. [CrossRef]
70. Asati, A.; Kaittanis, C.; Santra, S.; Perez, J.M. pH-Tunable Oxidase-Like Activity of Cerium Oxide Nanoparticles Achieving Sensitive Fluorigenic Detection of Cancer Biomarkers at Neutral pH. *Anal. Chem.* **2011**, *83*, 2547–2553. [CrossRef]
71. Ge, C.; Fang, G.; Shen, X.; Chong, Y.; Wamer, W.G.; Gao, X.; Chai, Z.; Chen, C.; Yin, J.-J. Facet energy versus enzyme-like activities: The unexpected protection of palladium nanocrystals against oxidative damage. *ACS Nano* **2016**, *10*, 10436–10445. [CrossRef]
72. Lin, L.; Song, X.; Chen, Y.; Rong, M.; Zhao, T.; Wang, Y.; Jiang, Y.; Chen, X. Intrinsic peroxidase-like catalytic activity of nitrogen-doped graphene quantum dots and their application in the colorimetric detection of H_2O_2 and glucose. *Anal. Chim. Acta* **2015**, *869*, 89–95. [CrossRef] [PubMed]
73. Wang, H.; Zheng, L.; Peng, C.; Guo, R.; Shen, M.; Shi, X.; Zhang, G. Computed tomography imaging of cancer cells using acetylated dendrimer-entrapped gold nanoparticles. *Biomaterials* **2011**, *32*, 2979–2988. [CrossRef] [PubMed]
74. Shah, V.; Shah, S.; Shah, H.; Rispoli, F.J.; McDonnell, K.T.; Workeneh, S.; Karakoti, A.; Kumar, A.; Seal, S. Antibacterial activity of polymer coated cerium oxide nanoparticles. *PLoS ONE* **2012**, *7*, e47827. [CrossRef] [PubMed]
75. Tian, J.; Liu, S.; Luo, Y.; Sun, X. Fe (III)-based coordination polymer nanoparticles: Peroxidase-like catalytic activity and their application to hydrogen peroxide and glucose detection. *Catal. Sci. Technol.* **2012**, *2*, 432–436. [CrossRef]
76. Song, Y.; Qu, K.; Zhao, C.; Ren, J.; Qu, X. Graphene Oxide: Intrinsic Peroxidase Catalytic Activity and Its Application to Glucose Detection. *Adv. Mater.* **2010**, *22*, 2206–2210. [CrossRef]
77. Lipinski, B. Hydroxyl Radical and Its Scavengers in Health and Disease. *Oxid. Med. Cell. Longev.* **2011**, *2011*, 809696. [CrossRef]
78. Frey, A.; Meckelein, B.; Externest, D.; Schmidt, M.A. A stable and highly sensitive 3,3′,5,5′-tetramethylbenzidine-based substrate reagent for enzyme-linked immunosorbent assays. *J. Immunol. Methods* **2000**, *233*, 47–56. [CrossRef]
79. Teodoro, K.B.R.; Migliorini, F.L.; Christinelli, W.A.; Correa, D.S. Detection of hydrogen peroxide (H_2O_2) using a colorimetric sensor based on cellulose nanowhiskers and silver nanoparticles. *Carbohydr. Polym.* **2019**, *212*, 235–241. [CrossRef]
80. Tian, R.; Zhang, B.; Zhao, M.; Zou, H.; Zhang, C.; Qi, Y.; Ma, Q. Fluorometric enhancement of the detection of H2O2 using different organic substrates and a peroxidase-mimicking polyoxometalate. *RSC Adv.* **2019**, *9*, 12209–12217. [CrossRef]
81. Chen, Y.; Zhong, Q.; Wang, Y.; Yuan, C.; Qin, X.; Xu, Y. Colorimetric detection of hydrogen peroxide and glucose by exploiting the peroxidase-like activity of papain. *RSC Adv.* **2019**, *9*, 16566–16570. [CrossRef]
82. Zhang, Z.; Liu, Q.; Liu, Y.; Qi, R.; Zhou, L.; Li, Z.; Yun, J.; Liu, R.; Hu, Y. Colorimetric H2O2 Detection Using Ag-Nanoparticle-Decorated Silica Microspheres. *Nano* **2020**, *15*, 2050009. [CrossRef]
83. Wang, Y.; Zhou, B.; Wu, S.; Wang, K.; He, X. Colorimetric detection of hydrogen peroxide and glucose using the magnetic mesoporous silica nanoparticles. *Talanta* **2015**, *134*, 712–717. [CrossRef] [PubMed]
84. Deutsch, J.C. Ascorbic Acid Oxidation by Hydrogen Peroxide. *Anal. Biochem.* **1998**, *255*, 1–7. [CrossRef] [PubMed]